JOURNAL OF GUIDANCE, CONTROL, AND DYNAMICS
Vol. 33, No. 1, January–February 2010

Analytical Study of the Primer Vector and Orbit Transfer Switching Function

Brian Roger Jamison* and Victoria Coverstone†
University of Illinois at Urbana–Champaign, Urbana, Illinois 61801-2957

DOI: 10.2514/1.41126

This work focuses on investigating the behavior of the orbit transfer switching function for the two-body problem. Recent work indicated that use of an analytical expression for the switching function could significantly reduce the computational time required to determine when to end coast arcs during trajectory optimization. This analysis of the switching function begins by showing how the primer vector and switching function in various coordinate systems are related, and two representative systems are considered for the remaining analysis. Given that multiple harmonics are manifest simultaneously in the switching function during coast arcs, some possible behaviors of such functions are considered relative to finding bounds containing the desired coast-terminating zero. It is seen that the method proposed in recent work can fail. A relatively simple improvement involving the slope of the switching function at the sampled points is used to make the method more robust and enable the production of example optimal solutions that would not have been possible with the earlier method. In terms of the two chosen systems, analytical expressions for the switching function and its derivative during coasting as well as transformation matrices that relate the systems to each other are therefore presented in Appendices A, B, and C.

Introduction

IN SOME mission scenarios, the assumption of Keplarian motion is sufficient during the early planning and optimization stage, and many spacecraft trajectory optimization software packages employ this relatively simple model of the two-body problem to speed up this initial process. Likewise, assuming Keplarian motion, former work has yielded analytical equations for the orbit transfer optimization costates during coast arcs [1,2]. Use of these analytic expressions as well as analytic equations for the states eliminates the inaccuracies and associated problem sensitivity that would otherwise be introduced by propagating the state and costate equations numerically. Also, the exact equations for the costates can be applied to the switching function (SF) to obtain an analytic expression for it during coasting arcs. Such an expression can be useful for accurate determination of coast-terminating switching times (zeros) and the associated states and costates in initial orbit planning software.

Given the complicated transcendental nature of the equation for the SF during coast arcs, solutions for its zeros are obtained by iterative methods. In such a process, it is critical to find the particular zero that terminates the given coast arc or, in other words, the first zero after the coast arc begins. Finding this coast-terminating zero (CTZ) is complicated by the fact that the equation for the SF during coasting can have multiple zeros over a single revolution, and these may even be arbitrarily close to each other. In an effort to take advantage of the analytic expression for the SF and thus reduce the computation time required for coast arcs, recent work by Xu [3] examined the analytic expression for the SF during coasting and determined what was called its maximum frequency. In that work, the results of the maximum frequency analysis were used to specify a fixed step size in an algorithm that would determine a set of bounds that would allegedly contain only the CTZ and no extraneous zeros of the SF. If correctly determined, such a set of bounds could then be provided to a zero finding algorithm (ZFA) to quickly and accurately determine the CTZ. For the two optimal orbit transfer cases considered in that work, it was reported that the computational time for the coast arcs with the proposed algorithm was 2.5 and 3.8% of the time required by a method that numerically propagated the trajectory during the coast arcs. Although the reported computational savings were significant, it is seen in this work that the method proposed therein can fail. This work reinvestigates the SF and presents an improvement that makes the method more robust.

Presented at the AAS/AIAA Astrodynamics Specialist Conference, Mackinac Island, MI, 19–23 August 2007; received 30 September 2008; revision received 6 July 2009; accepted for publication 7 July 2009.

*Graduate Research Assistant, Aerospace Engineering Department, 306 Talbot Laboratory, 104 South Wright Street; bjamiso2@illinois.edu.

†Professor, Aerospace Engineering Department, 306 Talbot Laboratory, 104 South Wright Street; vcc@illinois.edu. Associate Fellow AIAA.

Coordinate Systems and Optimal Control Theory

Two different coordinate systems will be used in this work. The first one uses the set of modified equinoctial orbit elements (MEOE) developed by Broucke and Cefola [4]. In terms of the classical orbit elements, semimajor axis a, eccentricity e, inclination i, longitude of the ascending node Ω, argument of periapse ω, and the true anomaly ν, these elements describe the orbit by the semilatus rectum:

$$p = a(1 - e^2) \tag{1}$$

as well as by

$$f = e\cos(\omega + \Omega) \tag{2}$$

$$g = e\sin(\omega + \Omega) \tag{3}$$

$$h = \tan(i/2)\cos\Omega \tag{4}$$

$$k = \tan(i/2)\sin\Omega \tag{5}$$

and

$$L = \nu + \Omega + \omega \tag{6}$$

where L is the true longitude. Thus, in the MEOE system, $\mathbf{x}_L = [\,p \quad f \quad g \quad h \quad k \quad L\,]^T$ will denote the state vector. Some benefits of the MEOE system are that the elements are free of singularities (except in the case where inclination $i = \pi$, which could be handled by a redefinition) and are also valid for parabolic and hyperbolic orbits. Equations of motion in this system were derived and tested for

a perturbation analysis of a highly eccentric orbit by Walker et al. [5]. The differential equations for the costates for this system were derived by Gao and Kluever [6], who used these coordinates for interplanetary trajectory optimization with a hybrid trajectory optimization method. These elements have also been successfully applied in other works [7].

The second coordinate system that will be used in this work is an eccentric longitude (EL) formulation that has been developed and tested by Kechichian [8]. In this system, which, for the captured orbits ($e < 1$) that will be studied here, is likewise free of singularities, the orbit size is defined in terms of a instead of p. The other orbit defining parameters are f, g, h, and k as defined in Eqs. (2–5). Finally, the fast variable is the eccentric longitude

$$F = E + \Omega + \omega \tag{7}$$

where E is the eccentric anomaly. Thus, the vector of states in the EL system will be denoted $\mathbf{x}_F = [\,a \quad f \quad g \quad h \quad k \quad F\,]^T$.

The relationships between the elements of the two coordinate systems are given by Eq. (1) and the fact that [9]

$$\tan\frac{E}{2} = \sqrt{\frac{1-e}{1+e}}\tan\frac{\nu}{2} \tag{8}$$

where $e = \sqrt{f^2 + g^2}$, which can be seen from Eqs. (2) and (3).

With the subscript A indicating that the quantity is in reference to some applicable coordinate system A (and similarly in the next section for B), denote the states by $\mathbf{x}_A$. The time rate of change of the states and the mass m of the spacecraft can be stated conveniently by the expressions

$$\dot{\mathbf{x}}_A = \mathbf{M}_A\left(\frac{T}{m}\boldsymbol{\alpha}\right) + \mathbf{D}_A \tag{9}$$

$$\dot{m} = -\frac{T}{gI_{\text{sp}}} \tag{10}$$

where $\mathbf{D}_A$ is a vector that gives the time rate of change of the states due to gravity, and $\mathbf{M}_A$ is a matrix that determines how the states change due to the thrust acceleration vector $(T/m)\boldsymbol{\alpha}$, where T is the magnitude of the thrust and $\boldsymbol{\alpha}$ is a unit vector pointing in the direction of the thrust acceleration.

The Hamiltonian plays an important role in formulating the optimal control problem and can be expressed as

$$H = \boldsymbol{\lambda}_A^T\mathbf{M}_A\frac{T}{m}\boldsymbol{\alpha} + \boldsymbol{\lambda}_A^T\mathbf{D}_A - \lambda_m\frac{T}{gI_{\text{sp}}} \tag{11}$$

where $\boldsymbol{\lambda}_A$ is a vector of costates corresponding to the states $\mathbf{x}_A$, and λ_m is the mass costate. For the MEOE system, the costates are denoted as $\boldsymbol{\lambda}_L = [\,\lambda_p^L \quad \lambda_f^L \quad \lambda_g^L \quad \lambda_h^L \quad \lambda_k^L \quad \lambda_L^L\,]^T$ and, for the EL system, they are denoted as $\boldsymbol{\lambda}_F = [\,\lambda_a^F \quad \lambda_f^F \quad \lambda_g^F \quad \lambda_h^F \quad \lambda_k^F \quad \lambda_F^F\,]^T$, where, as in [8], the superscript on individual costates is used to clarify which coordinate system it belongs to, because, for example, λ_f^L is, in general, not equal to λ_f^F. Once the Hamiltonian has been formed, the costates of the optimal control problem [10] are given by

$$\dot{\boldsymbol{\lambda}}_A = -\left(\frac{\partial H}{\partial \mathbf{x}_A}\right)^T = -\left(\boldsymbol{\lambda}_A^T\frac{\partial \mathbf{M}_A}{\partial \mathbf{x}_A}\frac{T}{m}\boldsymbol{\alpha} + \boldsymbol{\lambda}_A^T\frac{\partial \mathbf{D}_A}{\partial \mathbf{x}_A}\right)^T \tag{12}$$

$$\dot{\lambda}_m = -\frac{\partial H}{\partial m} = \boldsymbol{\lambda}_A^T\mathbf{M}_A\frac{T}{m^2}\boldsymbol{\alpha} \tag{13}$$

where boundary conditions are given in [10].

In the optimal control problem, it is desired to minimize the Hamiltonian with respect to all controls at all times. In doing this, first, the Pontryagin minimum principle is used such that the Hamiltonian is minimized with respect to the control angle by aligning it parallel to and in the opposite direction of $\boldsymbol{\lambda}_A^T\mathbf{M}_A$. Thus, because $\boldsymbol{\alpha}$ is a unit vector, using the superscript $*$ to indicate optimality, the optimal steering is given by

$$\boldsymbol{\alpha}^* = -\frac{[\boldsymbol{\lambda}_A^T\mathbf{M}_A]^T}{\|\boldsymbol{\lambda}_A^T\mathbf{M}_A\|} \tag{14}$$

Applying Eq. (14) to Eq. (11), the Hamiltonian is then written as

$$H = -\|\boldsymbol{\lambda}_A^T\mathbf{M}_A\|\frac{T}{m} + \boldsymbol{\lambda}_A^T\mathbf{D}_A - \lambda_m\frac{T}{gI_{\text{sp}}} \tag{15}$$

Now, to minimize the Hamiltonian with respect to all controls at all times, and because it is linear with respect to thrust magnitude, this minimization can be accomplished by forming the SF as

$$S = -\frac{\partial H}{\partial T} = \frac{\|\boldsymbol{\lambda}_A^T\mathbf{M}_A\|}{m} + \frac{\lambda_m}{gI_{\text{sp}}} \tag{16}$$

and assuming there are no singular arcs (where $S = 0$ for finite time), requiring

$$\begin{aligned} T &= 0 \quad \text{if } S < 0 \\ T &= T_{\max} \quad \text{if } S > 0 \end{aligned} \tag{17}$$

The case when $S = 0$ for finite time is not considered. Thus, the Hamiltonian could be rewritten as

$$H = -ST + \boldsymbol{\lambda}_A^T\mathbf{D}_A \tag{18}$$

which clearly shows that the Hamiltonian is minimized if the conditions given by Eq. (17) are true.

Noting [from Eqs. (10) and (13)] that the mass and mass costate are both constant during coasting, and because it will be used later, the derivative of the SF during coasting is derived here as

$$S' = \frac{(\boldsymbol{\lambda}_A^T\mathbf{M}_A)'(\boldsymbol{\lambda}_A^T\mathbf{M}_A)^T}{m\|\boldsymbol{\lambda}_A^T\mathbf{M}_A\|} \tag{19}$$

where the prime ($'$) notation indicates differentiation with respect to a specified fast variable. Note that, in addition to the application discussed later in this work, this derivative may be required in some ZFAs.

Coordinate Transformations and the Switching Function

It seems readily apparent that the times associated with the zeros of the SF expressed in one coordinate system will be the same as the times associated with the zeros of the SF expressed in any other coordinate system. However, because it is desirable to quickly and accurately determine the zeros of the SF, it will be advantageous to know more about the SF and to better understand its behavior. For example, it would be significant to know if the choice of coordinate system will change the nonzero behavior of the SF, particularly if that choice might give advantages (or disadvantages) in the zero search procedure. The question of how the chosen coordinate system will affect the behavior of the SF will therefore be addressed in this section. It will first be shown that, for this optimal control formulation, the value of the Hamiltonian [as represented by Eqs. (15) or (18)] is independent of the coordinate system used, from which it will follow that the SF has the same property. Then, because the SF may be written explicitly as a function of the angular position during coasting, a discussion about how various coordinate systems may result in equivalent zero search procedures will follow. From this discussion, it will become reasonable to reduce the number of coordinate systems that will be considered to two.

To show that the Hamiltonian at any given instant does not depend on the coordinate system chosen, first note that the term involving the mass costate does not depend on the coordinate system. To see that the other two terms in Eq. (15) are also independent of the coordinate system, first note the following relationship between time rates of change of the states of coordinate systems A and B, as specified by the chain rule and Eq. (9):

$$\dot{\mathbf{x}}_A = \frac{\mathrm{d}\mathbf{x}_A}{\mathrm{d}t} = \frac{\partial \mathbf{x}_A}{\partial \mathbf{x}_B}\frac{\mathrm{d}\mathbf{x}_B}{\mathrm{d}t} = \mathbf{R}_{AB}\left(\mathbf{M}_B\frac{T}{m}\boldsymbol{\alpha} + \mathbf{D}_B\right) = \mathbf{M}_A\frac{T}{m}\boldsymbol{\alpha} + \mathbf{D}_A \tag{20}$$

where $\mathbf{R}_{AB}$ is a Jacobian transformation matrix and is defined as

$$\mathbf{R}_{AB} \equiv \frac{\partial \mathbf{x}_A}{\partial \mathbf{x}_B} = \begin{bmatrix} \frac{\partial x_{A,1}}{\partial x_{B,1}} & \cdots & \frac{\partial x_{A,1}}{\partial x_{B,n}} \\ \vdots & \ddots & \vdots \\ \frac{\partial x_{A,n}}{\partial x_{B,1}} & \cdots & \frac{\partial x_{A,n}}{\partial x_{B,n}} \end{bmatrix} \tag{21}$$

where n is the number of coordinates (which is generally six, but could be four in the case of coplanar transfers). Note from Eq. (20) that premultiplying the equations of motion of coordinate system B by $\mathbf{R}_{AB}$ transforms them into the equations of motion of coordinate system A, as expressed by

$$\dot{\mathbf{x}}_A = \mathbf{R}_{AB}\dot{\mathbf{x}}_B \tag{22}$$

Setting $T = 0$ in Eq. (20), it is obvious that

$$\mathbf{R}_{AB}\mathbf{D}_B = \mathbf{D}_A \Rightarrow \mathbf{D}_B = \mathbf{R}_{AB}^{-1}\mathbf{D}_A \tag{23}$$

as long as the transformation matrix has full rank. Furthermore, by interchanging subscripts in Eq. (20), notice that

$$\mathbf{R}_{AB} = \mathbf{R}_{BA}^{-1} \tag{24}$$

Using the result of Eq. (23), it is seen from Eq. (20) that

$$\mathbf{R}_{AB}\left(\mathbf{M}_B\frac{T}{m}\boldsymbol{\alpha} + \mathbf{D}_B\right) = \mathbf{R}_{AB}\left(\mathbf{M}_B\frac{T}{m}\boldsymbol{\alpha}\right) + \mathbf{D}_A = \mathbf{M}_A\frac{T}{m}\boldsymbol{\alpha} + \mathbf{D}_A$$
$$\Rightarrow \mathbf{R}_{AB}\mathbf{M}_B = \mathbf{M}_A \tag{25}$$

Using this result, the interpretation of the Lagrange multipliers, and the chain rule,

$$\boldsymbol{\lambda}_A^T\mathbf{M}_A = \boldsymbol{\lambda}_A^T\mathbf{R}_{AB}\mathbf{M}_B = \frac{\partial J^*}{\partial \mathbf{x}_A}\frac{\partial \mathbf{x}_A}{\partial \mathbf{x}_B}\mathbf{M}_B = \frac{\partial J^*}{\partial \mathbf{x}_B}\mathbf{M}_B = \boldsymbol{\lambda}_B^T\mathbf{M}_B \tag{26}$$

where J^* is the optimal final cost. Notice from Eqs. (9) and (11) that, in the case where the states are the radius and velocity vectors, $\boldsymbol{\lambda}_A^T\mathbf{M}_A = \boldsymbol{\lambda}_\mathbf{v}$, the velocity costate vector, the negative of which Lawden [11] referred to as the primer vector. Thus, from Eq. (26), $\boldsymbol{\lambda}_A^T\mathbf{M}_A$ is the negative of the primer vector, and its magnitude and direction do not depend on the coordinate system. Now, in a similar manner as in Eq. (26),

$$\boldsymbol{\lambda}_A^T\mathbf{D}_A = \boldsymbol{\lambda}_A^T\mathbf{R}_{AB}\mathbf{D}_B = \boldsymbol{\lambda}_B^T\mathbf{D}_B \tag{27}$$

Thus, by substituting Eqs. (26) and (27) into Eq. (15), it becomes apparent that the value of the Hamiltonian at any given instant is independent of the coordinate system used. Because the SF [as written in Eq. (16)] is simply the negative of the derivative of the Hamiltonian with respect to the thrust magnitude, it follows that the value of the SF is also independent of the coordinate system. Also note that, because the primer vector is independent of the coordinate system chosen, applying Eq. (26) directly to Eq. (16) would provide an alternate proof of the same result.

Note from Eqs. (26) and (27) and that premultiplying the vector of costates in coordinate system B by $\mathbf{R}_{BA}^T$ transforms them into the costates in coordinate system A, as expressed by

$$\boldsymbol{\lambda}_A = \mathbf{R}_{BA}^T\boldsymbol{\lambda}_B \tag{28}$$

analogous to Eq. (22). Equation (28) can be helpful when costates are given relative to one coordinate system and are needed in another. An equivalent method for relating costates of different coordinate systems was used by Kechichian [8], and, in practice, could be used instead of Eq. (28) to transform the costates [because, in this work, the transformation matrices as derived will not be used to transform the equations of motion, as in Eq. (22)]. However, the derivation as it has been done earlier is helpful in this case because of the results expressed in Eqs. (26) and (27) and those discussed in the remainder of the paragraph following Eq. (27). Also, note that the results to this point are valid for both burn arcs and coast arcs. The transformation matrices between the MEOE and EL systems are presented in Appendix A. Also, for the MEOE system, the elements of $\mathbf{M}_L$ and $\mathbf{D}_L$ are given in Appendix B, and, for the EL system, the elements of $\mathbf{M}_F$ and $\mathbf{D}_F$ are given in Appendix C.

Before proceeding further relative to the SF and the coordinate system in which it is expressed, note that analytical equations in many coordinate systems (such as the Cartesian system) are usually given in terms of orbit elements (such as true anomaly). Furthermore, as noted by Kechichian [8], casting the trajectory optimization problem in an orbital element variational formulation is convenient because the boundary conditions are often given in these terms. For this reason, this study will employ orbital element variational coordinate systems.

There are many orbital element coordinate systems for which the variational equations have been derived. These either use classical elements or equinoctial formulations that eliminate singularities. Whereas the sixth element of the variational equations may take one of many forms, such as the mean, true, or eccentric anomaly or the corresponding longitudes, the variable on the right-hand side of the differential equations must be the true anomaly, eccentric anomaly, true longitude, or eccentric longitude [8]. Thus, casting the equations of motion in terms of mean anomaly, mean longitude, or time would require the extra step of solving Kepler's equation for the angular position. Casting the equations in terms of the true or eccentric anomaly or longitude has the benefit that, during coasting, the SF can be written as an explicit function of that angular fast variable, allowing for direct computation of the SF, with the corresponding time being analytically calculated from Kepler's equation as needed. For these reasons, only coordinate systems that use true or eccentric fast variables (anomaly and longitude) will be employed in this work.

Now, although it has been shown that the value of the SF at a given time will not depend on the coordinate system chosen, this does not mean that all coordinate systems will result in equivalent zero search procedures. This is because, for noncircular orbits, the rate of change for true fast variables is not equal to the rate of change in eccentric fast variables, corresponding to the fact that eccentric fast variables lag true fast variables as the spacecraft travels from periapse to apoapse and lead them as the spacecraft travels from apoapse to periapse. Furthermore, this means that the slope of the SF (as well as higher-order derivatives) with respect to true fast variables will not be identical to that for eccentric fast variables, resulting in different zero search procedures either by a particular bounds search method with a fixed step size or within a particular ZFA.

However, from Eqs. (6) and (7), it can be seen that during coasting there is a linear relationship between each anomaly and the corresponding longitude because ω and Ω are constants under Keplarian motion. If the anomaly (e.g., true or eccentric) is denoted ξ and the corresponding longitude is denoted

$$\gamma = \xi + \Omega + \omega \tag{29}$$

the SF as a function of the longitude can be denoted by $S(\gamma) = S(\xi + \Omega + \omega)$. Thus, the SF in terms of the longitude is simply translated along the abscissa an amount $\Omega + \omega$ relative to the SF in terms of the anomaly. Furthermore, because Ω and ω are constants during coasting,

$$\mathrm{d}\gamma = \mathrm{d}\xi \tag{30}$$

from which it follows that rates of change of the anomaly and the longitude are equal. Another way of saying this is that the shape of the plot of the SF during coasting is the same in terms of either the anomaly or the corresponding longitude and the only difference is the positioning along the abscissa. Thus, the bounds search procedure beginning at the initial ξ or the corresponding γ will be the same for a coordinate system given in terms of either the anomaly or the longitude as long as the sampling rate is the same. Furthermore, the

preceding facts mean that, within any given ZFA, the search procedure for the two coordinate systems represented by ξ and γ will be identical as long as the corresponding bounds and the corresponding initial values of anomaly and longitude are used.

From the preceding results it is sensible to reduce the number of coordinate systems studied to two. In summation, the reasons for choosing the MEOE and EL systems for this work are that 1) the SF can be written explicitly in terms of the fast variable of either system and these systems do not require the solution of Kepler's equation for the angular position, 2) both are free of singularities that exist in other coordinate systems, 3) both are given in terms of orbital elements, which makes the boundary conditions easy to define, and 4) all other coordinate systems that employ a true or eccentric fast variable will result in equivalent zero search procedures as the MEOE and EL systems, respectively.

With the preceding in mind, it is worthwhile to note that, in the work by Xu [3] (which will be further considered in the remainder of this work), the SF was cast in terms of the velocity costate vector (the negative of the primer vector) with terms written as functions of true anomaly. Therefore, the SF as written in that work is essentially equivalent to the SF written in this work in terms of MEOE variables.

Analysis of the Switching Function During Coasting and Multiharmonic Functions

Equations for the costates and/or the SF during coasting have been derived in many coordinate systems in other works [1–3,12]. Appendices B and C contain equations for the costates and the SF in terms of the MEOE and EL coordinate systems, respectively, as derived in [12]. Appendix B also shows quantities necessary for calculation of the derivative of the SF with respect to true longitude, as does Appendix C for the derivative with respect to eccentric longitude. Verifications of the results in the Appendices are discussed in [12].

As a first step in this analysis, note that, where η is a strictly positive integer, the greatest possible number of zeros over any length 2π interval (GPNZ2PI) for $\sin \eta x$ and $\cos \eta x$ (including both endpoints) is $2\eta + 1$. It may also be noted that, if $f(x)$ is a strictly increasing (or strictly decreasing) function of x, $f(x) \sin \eta x$ and $f(x) \cos \eta x$ have the same zeros as $\sin \eta x$ and $\cos \eta x$, respectively, and an additional one where $f(x) = 0$ if this location does not correspond to a zero of the periodic part. Now, for the EL coordinate system, the GPNZ2PI for the primer vector and SF (which is composed of terms and products of quantities of the forms $\sin x$, $\cos x$, $x \sin x$, and $x \cos x$) may be calculated by combining quantities while applying the rules (considering that constants contribute no zeros) [3]: 1) the GPNZ2PI of a sum is the largest GPNZ2PI of the individual terms, and 2) the GPNZ2PI of a product is calculated by summing the GPNZ2PI of the two factors and then subtracting one (if the GPNZ2PI of both terms is nonzero).

In calculating the GPNZ2PI of the primer vector and SF, note that, in the EL system, the oscillatory quantity

$$b = 1 - f \cos F - g \sin F = 1 - e \cos E \tag{31}$$

appears in the denominator of several terms. However, because b is both finite and strictly positive for the captured orbits (where $0 \leq e < 1$ such that $0 < b < 2$) considered in this paper, division by this term will have no effect on the number of zeros of the primer vector or SF.

Now, as explained in Appendix C, in the EL coordinate system, during coasting, it is convenient to write

$$\boldsymbol{\lambda}_F^T \mathbf{M}_F = \boldsymbol{\lambda}_{F,o}^T \mathbf{N}_F \tag{32}$$

where $\boldsymbol{\lambda}_{F,o}$ is the vector of initial costates, and the elements of $\mathbf{N}_F$ are given in Appendix C. Thus, the coast arc primer vector can be written as a linear combination of the elements of $\mathbf{N}_F$, which are themselves formed by linear combinations of the quantities X_1, Y_1, $\dot{X}_1$, $\dot{Y}_1$, $\partial X_1/\partial f$, $\partial X_1/\partial g$, $\partial Y_1/\partial f$, $\partial Y_1/\partial g$, $Q_{X,0}$, and $Q_{Y,0}$ (which are also given in Appendix C). The GPNZ2PI of these quantities and the resulting GPNZ2PI for the nonzero elements of $\mathbf{N}_F$ are shown in Table 1. With these results, and following the procedure outlined earlier, the GPNZ2PI of the coast arc primer vector is five, and thus the GPNZ2PI of the SF is nine (note that taking the square root is assumed to not change the GPNZ2PI in this case). With the proof in the preceding section that the value of the SF is independent of the coordinate system chosen, it is concluded that there will be no more than nine zeros over any interval of the SF of length 2π, regardless of the coordinate system chosen.

Table 1 GPNZ2PI for quantities in the EL coast arc primer vector and SF

GPNZ2PI	Quantities
3	$X_1, Y_1, \dot{X}_1, \dot{Y}_1, N_{11}^F, N_{12}^F, N_{23}^F, N_{33}^F, N_{43}^F, N_{53}^F, N_{63}^F$
5	$\partial X_1/\partial f, \partial X_1/\partial g, \partial Y_1/\partial f, \partial Y_1/\partial g, Q_{X,0}, Q_{Y,0}, N_{21}^F, N_{31}^F, N_{61}^F, N_{22}^F, N_{32}^F, N_{62}^F$

In [3], based on the conclusion that there would be a maximum of 17 zeros in each interval of length 2π, it was concluded to sample values of the SF at 17 uniformly distributed values of true anomaly (i.e., every $\pi/8$ rad) over one orbit starting at the beginning of the coast. For the now concluded GPNZ2PI of nine, one might likewise choose to sample the SF at intervals of length $\pi/4$ rad. Apparently, the choice of sampling rate was made because it was assumed that the SF would behave something like an ordinary sinusoid, and it was unfortunately concluded that the SF between each of the sampled locations "is monotonic and includes a maximum of one zero." (Note that this would imply that any local maxima or minima would be among the sampled points.) It was then concluded that finding bounds containing only the coast-terminating zero would simply be a matter of finding the first change in sign of the SF as the sampled points were evaluated from left to right. Such a bounds determination method will hereafter be referred to as fixed-step-value-only sampling (1-FSVOS).

Now, whereas behavior similar to an ordinary sinusoid might occur in some cases, this will not always be the case because of the various harmonics extant in the SF, the combined effects of which can make the behavior more complicated. As a demonstration of such a case, consider the function $f_0(x) = 2 \sin x + (1 + \Delta) \sin 2x$ over the range $[0, 2\pi]$. This function is shown in Fig. 1 for $\Delta = 0, 0.2, 0.4$. Its derivative is $f_0'(x) = 2 \cos x + 2(1 + \Delta) \cos 2x$. Because the largest frequency of $f_0(x)$ is two, it will have no more than five zeros over the specified range, three of which will always be located at zero, π, and 2π rad. Note that $f_0'(0) = f_0'(2\pi) = 4 + 2\Delta$ and $f_0'(\pi) = 2\Delta$, so that, if $\Delta < -2$ or $\Delta > 0$, the slope at these three locations will have the same sign, indicating that there are two more zeros, one of each of which will be located on either side of the zero at π rad, with the particular locations depending on Δ. Using a double-angle formula and letting $x = \pi + \delta x$, these other two zeros are found to be located at $x = \pi \pm \delta x$ rad, where $\delta x = \cos^{-1}[1/(1 + \Delta)]$. Also in Fig. 1, δx is plotted vs Δ, from which it can be seen that the nonfixed zeros can be located arbitrarily close to $x = \pi$ rad as Δ approaches zero from above. Consider the case where the zero at $x = \pi - \delta x$ is seen as a coast-initiating zero, and the zero at π rad is seen as the corresponding CTZ. For a fixed-step-size sampling scheme, regardless of how small of a step size chosen, there will always be a value of Δ such that $2\delta x$ (the distance to what might be considered the next coast-initiating zero) is smaller, which would result in the correct CTZ not being detected. Thus, with multiple harmonics in a function, the behavior can become more complicated and result in sets of zeros being arbitrarily close to each other, making them difficult (if not impossible) to detect by sampling methods which use a fixed step size.

To further examine possible behaviors of multiharmonic functions and the challenge of accurately determining the CTZ, providing context for discussion of a possible method of solution, consider the simple oscillatory function

$$f_1(x) = \cos x - \cos 1 \sin 2x + \sin 1 \cos 2x \tag{33}$$

Note that two different frequencies will be manifest in this function because the first term has a frequency of one and the other two terms have a frequency of two. Thus, the GPNZ2PI for $f_1(x)$ is five.

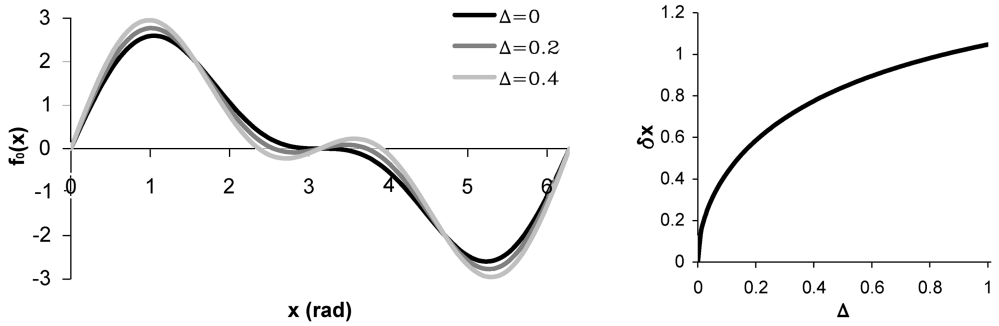

Fig. 1 Plots of $f_0(x)$ for $\Delta = 0, 0.2, 0.4$ (left), and $\delta x = \cos^{-1}[1/(1+\Delta)]$ (right).

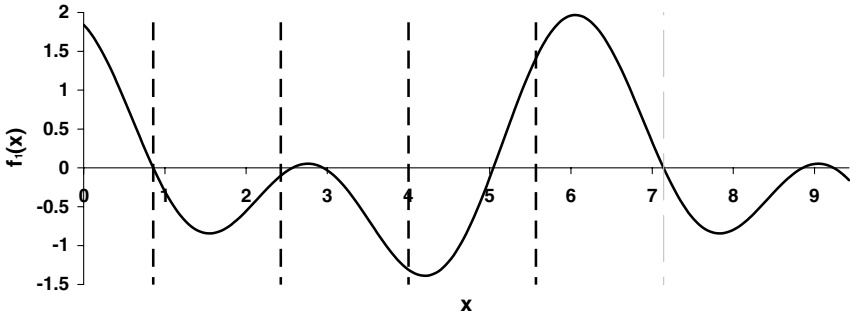

Fig. 2 Plot of $f_1(x)$. Dashed lines are located where sampling will take place.

Figure 2 shows this function over $[0, 3\pi]$. If the zero located at approximately $x = 0.85$ rad is seen as the coast-initiating zero, for a 1-FSVOS scheme with a corresponding step size of $\pi/2$ (5/period), the function would be sampled at the locations indicated by the darker vertical lines (from left to right) before a change in sign would be detected. The resulting bounds provided to a ZFA would be the sampled locations on either side of the zero at approximately 5 rad instead of those containing the CTZ of approximately $x = 2.6$ rad (as well as an additional zero at approximately $x = 3$ rad).

Although a higher sampling rate might solve this problem in some cases, it has already been seen in the case of $f_0(x)$ that this will, in general, not always be the case. Another option, which would solve the problem for $f_1(x)$ (but not for $f_0(x)$), is to also check the value of the derivative at each of the sampled locations. If the slope of the function changes from positive to negative from one sampling point to the next, a point between these two points where the slope is equal to zero represents a maximum value of the function in that range. Such a point could be found and, if the value of the function at this point were positive, it would represent an upper bound for the ZFA, whereas the preceding point would represent a lower bound. In the case of $f_1(x)$, this would not only lead to the detection of the sign change in the function, but also reduce the bounds for the zero search such that they would contain only the CTZ, and not the additional zero. This more robust scheme will be referred to as fixed-step value and slope sampling (2-FSVSS). Although this method may also fail in cases such as $f_0(x)$, where a short coast is followed by a short burn signal and then another coast, this represents an improvement over 1-FSVOS, which can fail in the case of a relatively long coast followed by a short burn signal and another coast, which in practice includes many optimal trajectories having both near impulsive burns as well as relatively short continuous burns.

Optimal Trajectory Examples

Example trajectories will now be considered which will employ and compare the results from 1-FSVOS and 2-FSVSS for the process of determining CTZs for the SF. For the optimal trajectory examples that follow, the solutions were obtained using MATLAB with a shooting method that employed the `fmincon` function to iterate on the initial values and ensure that the final constraints were satisfied. For burn arcs, the differential equations for the MEOE system as outlined in [6] were numerically integrated. Over coast arcs, 1-FSVOS and 2-FSVSS were used (with any failures to concur being noted) with sampling intervals of $\pi/8$ and $\pi/6$ rad for the MEOE system and at $\pi/6$ and $\pi/4$ rad for the EL system. Note that the elapsed time at the sampled values of the longitudes was calculated from Kepler's equation and, if it was greater than the remaining time, the angular position at the final time was iteratively calculated by using the Laguerre–Conway algorithm [9,13]. (Note that this can help reduce the chance of not detecting a zero because it effectively reduces the step size of the last step.[‡])

The first example will be considered a minimum-propellant transfer from the circularized orbit of Earth to the circularized orbit of Mars (similar to the Bryson and Ho [10] problem) where the time of flight is fixed at 1 year. The problem is posed in canonical units and the orbit parameters are listed in Table 2. In canonical units, the initial mass of the spacecraft is one, and 2π time units are equal to 1 year such that the gravitational parameter is unity. For the interpretation where the initial mass of the spacecraft is equal to 4536 kg, the thrust is approximately 3.781 N and the mass flow rate is approximately 6.772×10^{-5} kg/s. Figure 3 shows the optimal trajectory in this case. For this trajectory, about 9.54% of the initial mass is required as fuel.

Now, for the two coordinate systems used and the sampling intervals used in each, Table 3 indicates whether or not the CTZ was detected by 1-FSVOS for this trajectory. For this first example, the SF is plotted against eccentric longitude in Fig. 3. In the figure, sampled values of the SF at intervals of $\pi/6$ rad are indicated by dots. From this, it can be seen that no samples occurred in the region where the final burn is signaled, as is indicated in Table 3. Thus, for the EL system and for 1-FSVOS at this rate, the zero at the beginning of the final burn would not have been detected and the algorithm would not have been able to converge to the optimal solution. This was also the case with the larger intervals for both coordinate systems. However, for the cases listed in Table 3, the zero was detected when 2-FSVSS was used.

Now, consider the case of the 1 year transfer as before except with a targeted final eccentricity equal to the eccentricity of the actual orbit of Mars, $e_f = 0.0934$. The propellant mass required for this transfer

[‡]If this was done in [3], it may have contributed to the detection of the appropriate zeros in the examples considered therein.

Table 2 Orbit parameters for the coplanar orbit transfer shown in Fig. 3

	a, AU	e	i	Ω	ω	ν
Initial	1	0	0	0	0	0
Target	1.5237	0	0	0	0	Free

was about 9.40% of the spacecraft's initial mass. The optimal transfer is roughly the same as before and is seen in Fig. 4. Figure 4 also shows the SF for this transfer plotted vs the true longitude, with dots indicating the sampling locations when a $\pi/8$ rad sampling interval was used. It may be noted that this is the sampling interval espoused in [3], and, as explained earlier, the coordinate system is equivalent to that used in the same work as well. As seen in the figure and as indicated in Table 3, if 1-FSVOS is used, the zero at the beginning of the final burn would not have been identified, thus preventing the attainment of the optimal solution. However, as in the previous case, when 2-FSVSS is used, the correct zero was detected for all of the cases given in Table 3.

Table 3 Results of sampling intervals used for examples

		Zero detected by value sampling alone?	
Coordinate system	Sampling interval, rad	Circular final orbit	Eccentric final orbit
MEOE	$\pi/8$	Yes	No
	$\pi/6$	No	No
EL	$\pi/6$	No	Yes
	$\pi/4$	No	Yes

In concluding these examples, it should be noted that, whereas 1-FSVOS would have failed in the majority of these cases, even when

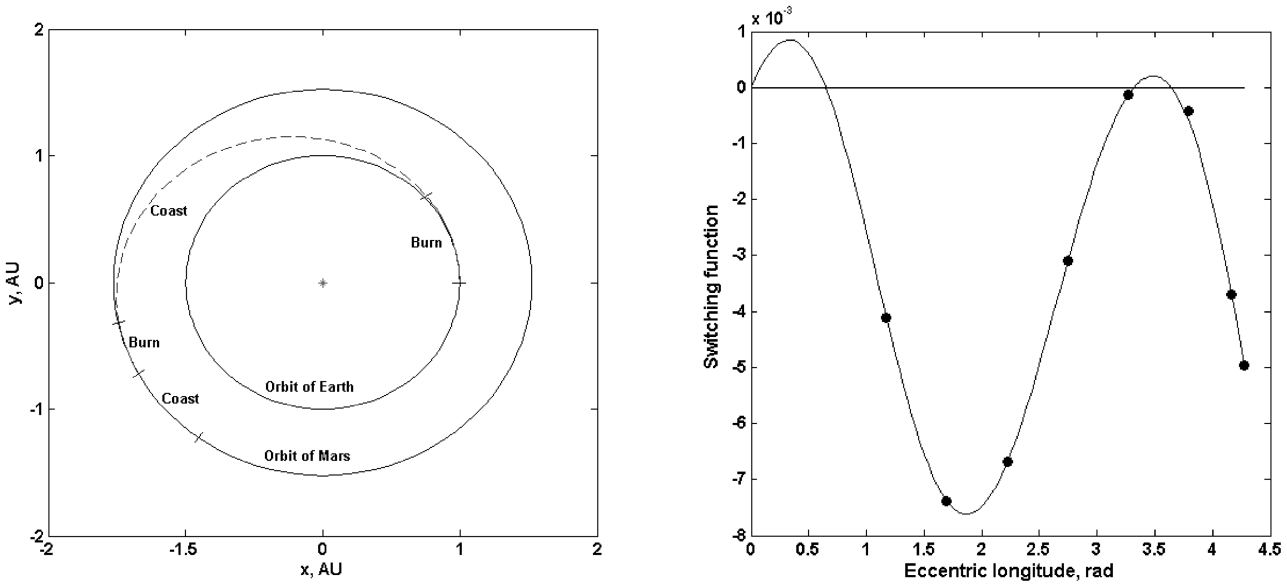

Fig. 3 Plots of trajectory (left) and accompanying SF vs eccentric longitude for transfer from Earth orbit to circular Mars orbit with a sampling interval of $\pi/6$ indicated (right).

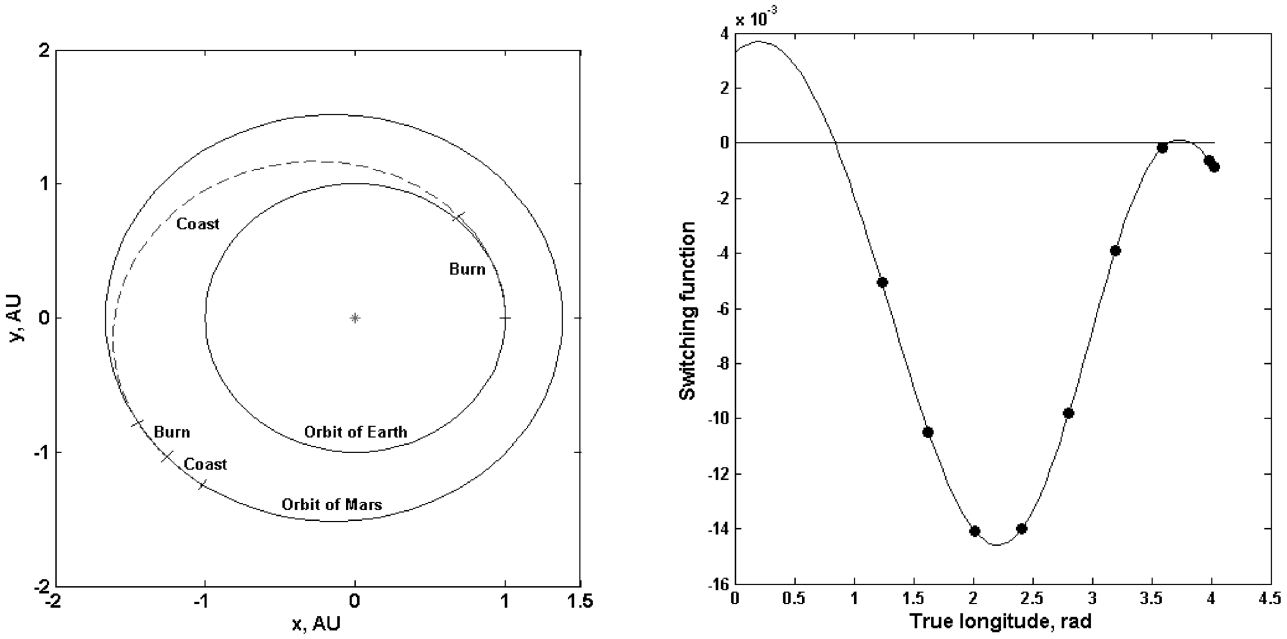

Fig. 4 Plots of trajectory (left) and corresponding SF vs true longitude for transfer from Earth orbit to eccentric Mars orbit with a sampling interval of $\pi/8$ indicated (right).

larger sampling intervals were used, convergence to the optimal solution was attained when 2-FSVSS was used.

Now, although 2-FSVSS was successfully used to produce the preceding examples and shows improvement over 1-FSVOS, as indicated in this paper, it may fail in cases where a short coast is followed by a short burn signal and then another coast. It was seen that analogous cases could exist for $f_o(x)$, where the fixed size sampling interval may not always work as it did in the optimal trajectories considered. Although it is conceivable that such cases (and perhaps other malignant ones) may be encountered during the optimization process, it seems that the majority of optimal trajectories in practice will be more benign, as in the ones considered herein. (Further, note that an indication of a long thrust arc after any coast arc, such as is often the case for many modern low-thrust trajectories, will reduce or even eliminate the chance of the preceding CTZ being undetected by either method.) In any case, given the shortcomings of fixed-step-size sampling, a better option may be to use an adjustable step size (although this was not attempted in this work). If this is done [perhaps using a method that checks the slope (and possibly higher-order derivatives) to help determine an appropriate step size], the derivations in the Appendices will be valuable.

Conclusions

An in-depth analysis of the switching function has been performed to gain a better understanding of its behavior, especially during coast arcs. Equations were derived to show that the primer vector and the switching function are independent of the coordinate system used, thus making conclusions in this work applicable in many coordinate systems. Exact equations for the costates during coasting were derived and used to form analytical expressions for the switching function in two coordinate systems. Additionally, as made useful by the method proposed, derivatives of the switching function were derived in both of the coordinate systems. The equations for the primer vector and the switching function in terms of the eccentric longitude system were analyzed to show that the number of zeros in any interval of length 2π of the switching function is no greater than nine, which is less than the previously published maximum of 17. Some possible behaviors of functions manifesting multiple frequencies were considered and the results were used to propose a more robust method for sampling the switching function during coasting. This method involves checking the slope of the switching function at the sampled points and finding a maximum value between points when the slope of the switching function changes from positive to negative from one sampled point to the next. Examples were given of cases where the new sampling algorithm enabled trajectories to be optimized, whereas a previously proposed algorithm would have failed.

Appendix A: Transformation Matrices

Noting that the eccentric longitude system is only valid for elliptical orbits ($e < 1$), the orbit size elements of the modified equinoctial orbit elements and EL systems are related by Eqs. (1–3) as

$$p = a(1 - f^2 - g^2) \tag{A1}$$

which can be rewritten as

$$a = p/(1 - f^2 - g^2) \tag{A2}$$

Also, using Eqs. (2), (3), (6), and (7) in Eq. (8), the true longitude can be written in terms of EL variables and the eccentric longitude in terms of MEOE variables, respectively, as

$$L = 2\tan^{-1}\left[\sqrt{\frac{1+\sqrt{f^2+g^2}}{1-\sqrt{f^2+g^2}}}\tan\left(\frac{F-\tan^{-1}(g/f)}{2}\right)\right] + \tan^{-1}(g/f) \tag{A3}$$

$$F = 2\tan^{-1}\left[\sqrt{\frac{1-\sqrt{f^2+g^2}}{1+\sqrt{f^2+g^2}}}\tan\left(\frac{L-\tan^{-1}(g/f)}{2}\right)\right] + \tan^{-1}(g/f) \tag{A4}$$

Noting the preceding relationships between the variables of the two coordinate systems, from Eq. (21), transformation matrices between the MEOE and EL systems are

$$\mathbf{R}_{LF} = \begin{bmatrix} \frac{\partial p}{\partial a} & \frac{\partial p}{\partial f} & \frac{\partial p}{\partial g} & 0 & 0 & 0 \\ 0 & 1 & 0 & 0 & 0 & 0 \\ 0 & 0 & 1 & 0 & 0 & 0 \\ 0 & 0 & 0 & 1 & 0 & 0 \\ 0 & 0 & 0 & 0 & 1 & 0 \\ 0 & \frac{\partial L}{\partial f} & \frac{\partial L}{\partial g} & 0 & 0 & \frac{\partial L}{\partial F} \end{bmatrix} \tag{A5}$$

$$\mathbf{R}_{FL} = \begin{bmatrix} \frac{\partial a}{\partial p} & \frac{\partial a}{\partial f} & \frac{\partial a}{\partial g} & 0 & 0 & 0 \\ 0 & 1 & 0 & 0 & 0 & 0 \\ 0 & 0 & 1 & 0 & 0 & 0 \\ 0 & 0 & 0 & 1 & 0 & 0 \\ 0 & 0 & 0 & 0 & 1 & 0 \\ 0 & \frac{\partial F}{\partial f} & \frac{\partial F}{\partial g} & 0 & 0 & \frac{\partial F}{\partial L} \end{bmatrix} \tag{A6}$$

From Eq. (A1),

$$\frac{\partial p}{\partial a} = 1 - f^2 - g^2, \qquad \frac{\partial p}{\partial f} = -2af, \qquad \frac{\partial p}{\partial g} = -2ag \tag{A7}$$

From Eq. (A2),

$$\frac{\partial a}{\partial p} = 1/(1 - f^2 - g^2), \qquad \frac{\partial a}{\partial f} = 2fa\frac{\partial a}{\partial p}, \qquad \frac{\partial a}{\partial g} = 2ga\frac{\partial a}{\partial p} \tag{A8}$$

To simplify the derivation of the partial derivatives of Eq. (A3), define

$$L_1 = 2\tan^{-1}\left[\sqrt{\frac{1+e}{1-e}}\tan\left(\frac{F-L_2}{2}\right)\right] \tag{A9}$$

where L_2 is defined as

$$L_2 = \tan^{-1}\left(\frac{g}{f}\right) \tag{A10}$$

so that $L = L_1 + L_2$. Also define

$$L_3 = \sqrt{\frac{1+\sqrt{f^2+g^2}}{1-\sqrt{f^2+g^2}}} = \sqrt{\frac{1+e}{1-e}} \tag{A11}$$

and

$$L_4 = \tan\left(\frac{F-\tan^{-1}(g/f)}{2}\right) = \tan\left(\frac{F-L_2}{2}\right) \tag{A12}$$

such that $L_1 = 2\tan^{-1}(L_3L_4)$. Thus,

$$\frac{\partial L}{\partial y} = \frac{\partial L_1}{\partial y} + \frac{\partial L_2}{\partial y} \tag{A13}$$

where $y = f, g, F$. Now,

$$\frac{\partial L_1}{\partial y} = 2\frac{1}{1+(L_3L_4)^2}\left(L_3\frac{\partial L_4}{\partial y} + \frac{\partial L_3}{\partial y}L_4\right) \tag{A14}$$

$$\frac{\partial L_2}{\partial f} = \frac{-g}{f^2+g^2}, \qquad \frac{\partial L_2}{\partial g} = \frac{f}{f^2+g^2}, \qquad \frac{\partial L_2}{\partial F} = 0 \tag{A15}$$

where $e \neq 0$, and also

$$\frac{\partial L_3}{\partial f} = \frac{1}{(1-e)^2 L_3}\frac{f}{e}, \qquad \frac{\partial L_3}{\partial g} = \frac{1}{(1-e)^2 L_3}\frac{g}{e}, \qquad \frac{\partial L_3}{\partial F} = 0 \tag{A16}$$

$$\frac{\partial L_4}{\partial f} = -\frac{1+L_4^2}{2}\frac{\partial L_2}{\partial f}, \qquad \frac{\partial L_4}{\partial g} = -\frac{1+L_4^2}{2}\frac{\partial L_2}{\partial g}$$
$$\frac{\partial L_4}{\partial F} = \frac{1+L_4^2}{2} \tag{A17}$$

It can be shown that

$$\lim_{e\to 0}\frac{\partial L}{\partial f} = \sin F, \qquad \lim_{e\to 0}\frac{\partial L}{\partial g} = -\cos F, \qquad \left.\frac{\partial L}{\partial F}\right|_{e=0} = 1 \tag{A18}$$

and so the right-hand side of these expressions may be used in place of Eq. (A13) when $e = 0$, so that the elements of the transformation matrix are defined at this point.

Likewise, in finding the partial derivatives of Eq. (A4), define

$$F_1 = 2\tan^{-1}\left[\sqrt{\frac{1-e}{1+e}}\tan\left(\frac{L-F_2}{2}\right)\right] \tag{A19}$$

where

$$F_2 = \tan^{-1}(g/f) = L_2 \tag{A20}$$

so $F = F_1 + F_2$. Also, define

$$F_3 = \sqrt{\frac{1-\sqrt{f^2+g^2}}{1+\sqrt{f^2+g^2}}} = \sqrt{\frac{1-e}{1+e}} = \frac{1}{L_3} \tag{A21}$$

and

$$F_4 = \tan\left(\frac{L-\tan^{-1}(g/f)}{2}\right) = \tan\left(\frac{L-F_2}{2}\right) \tag{A22}$$

such that $F_1 = 2\tan^{-1}(F_3 F_4)$. Therefore,

$$\frac{\partial F}{\partial z} = \frac{\partial F_1}{\partial z} + \frac{\partial F_2}{\partial z} \tag{A23}$$

where $z = f, g, L$. Similar to Eqs. (A14) and (A15),

$$\frac{\partial F_1}{\partial z} = 2\frac{1}{1+(F_3F_4)^2}\left(F_3\frac{\partial F_4}{\partial z} + \frac{\partial F_3}{\partial z}F_4\right) \tag{A24}$$

$$\frac{\partial F_2}{\partial f} = \frac{\partial L_2}{\partial f} = \frac{-g}{f^2+g^2}, \qquad \frac{\partial F_2}{\partial g} = \frac{\partial L_2}{\partial g} = \frac{f}{f^2+g^2}, \qquad \frac{\partial F_2}{\partial L} = 0 \tag{A25}$$

where $e \neq 0$ as before, and also

$$\frac{\partial F_3}{\partial f} = \frac{-1}{(1+e)^2 F_3}\frac{f}{e}, \qquad \frac{\partial F_3}{\partial g} = \frac{-1}{(1+e)^2 F_3}\frac{g}{e}, \qquad \frac{\partial F_3}{\partial L} = 0 \tag{A26}$$

$$\frac{\partial F_4}{\partial f} = -\frac{1+F_4^2}{2}\frac{\partial F_2}{\partial f}, \qquad \frac{\partial F_4}{\partial g} = -\frac{1+F_4^2}{2}\frac{\partial F_2}{\partial g}$$
$$\frac{\partial F_4}{\partial L} = \frac{1+F_4^2}{2} \tag{A27}$$

However, similar to Eq. (A18), it can be shown that

$$\lim_{e\to 0}\frac{\partial F}{\partial f} = -\sin L, \qquad \lim_{e\to 0}\frac{\partial F}{\partial g} = \cos L, \qquad \left.\frac{\partial F}{\partial L}\right|_{e=0} = 1 \tag{A28}$$

As noted earlier, the right-hand sides of these expressions can be used in place of Eq. (A23) when $e = 0$, so that the transformation matrix is defined at this point. It should be noted that this result and that in Eq. (A18) are corrections of the associated conference paper (noted at the beginning of this paper) as well as the thesis [12], where, due to the first two expressions in both of Eqs. (A15) and (A25), it had been assumed that Eqs. (A13) and (A23) were indeterminate when $e = 0$.

A final note of interest is that the equations relating the costates in one coordinate system to the costates in the other coordinate system can be derived from properties of a canonical transformation, as was done by Kechichian [8].

Appendix B: Modified Equinoctial Orbit Elements System Equations

Prime ($'$) notation will be used extensively in Appendices B and C and denotes differentiation with respect to the relevant fast variable, and so in this Appendix it implies differentiation with respect to the true longitude L. Also, because the equations considered in this and the next Appendix are relevant to Keplarian motion, differentiation will only be with respect to the applicable fast variable. The derivations that lead to the equations in both this and the next appendix can be seen in greater detail in [12].

For the MEOE coordinate system, the matrices $\mathbf{M}_L$ and $\mathbf{D}_L = [0 \quad 0 \quad 0 \quad 0 \quad 0 \quad D_L^L]^T$ are given in [6], and the nonzero elements are rewritten here as

$$M_{21}^L = \sqrt{\frac{p}{\mu}}\sin L, \qquad M_{31}^L = -\sqrt{\frac{p}{\mu}}\cos L, \qquad M_{12}^L = \sqrt{\frac{p}{\mu}}\frac{2p}{w}$$
$$M_{22}^L = \sqrt{\frac{p}{\mu}}\left(\cos L + \frac{\cos L + f}{w}\right)$$
$$M_{32}^L = \sqrt{\frac{p}{\mu}}\left(\sin L + \frac{\sin L + g}{w}\right), \qquad M_{23}^L = -gM_{63}^L$$
$$M_{33}^L = fM_{63}^L \qquad M_{43}^L = \sqrt{\frac{p}{\mu}}\frac{s^2}{2w}\cos L, \qquad M_{53}^L = \sqrt{\frac{p}{\mu}}\frac{s^2}{2w}\sin L$$
$$M_{63}^L = \sqrt{\frac{p}{\mu}}\frac{h\sin L - k\cos L}{w}, \qquad D_L^L = \sqrt{\frac{\mu}{p^3}}w^2 \tag{B1}$$

where $w = 1 + f\cos L + g\sin L$ and $s^2 = 1 + h^2 + k^2$ as in [6]. For notational convenience, the derivative of w with respect to true longitude is denoted $w' = -f\sin L + g\cos L$.

During coast arcs, the equations for the MEOE costates are (defining $j \equiv \sqrt{1-e^2}$),

$$\lambda_p^L = \lambda_{p,o}^L + \lambda_{L,o}^L\frac{3}{2}\frac{w_o^2}{pj^3}(\Lambda_p - \Lambda_{p,o})$$
$$\lambda_f^L = \lambda_{f,o}^L - \lambda_{L,o}^L\frac{w_o^2}{j^5}(\Lambda_f - \Lambda_{f,o})$$
$$\lambda_g^L = \lambda_{g,o}^L - \lambda_{L,o}^L\frac{w_o^2}{j^5}(\Lambda_g - \Lambda_{g,o})$$
$$\lambda_h^L = \lambda_{h,o}^L, \qquad \lambda_k^L = \lambda_{k,o}^L, \qquad \lambda_L^L = \lambda_{L,o}^L\left(\frac{w_o}{w}\right)^2 \tag{B2}$$

where

$$\Lambda_p = E + \frac{w'j}{w}$$

$$\Lambda_f = -3fE + \frac{j}{w^2}[(\cos L - 2f)ww' + (g + \sin L)(j^2 + w^2)]$$

$$\Lambda_g = -3gE + \frac{j}{w^2}[(\sin L - 2g)ww' - (f + \cos L)(j^2 + w^2)] \tag{B3}$$

and the subscript o denotes the initial value of the particular quantity. Noting from Eq. (13) that the mass costate is constant during coasting, the equation for the SF during coasting is easily formed from Eq. (16) using the costates and the matrix $\mathbf{M}_L$ as given earlier.

For the proposed method of checking the slope at each sampled point, the derivatives with respect to true longitude of the SF are now calculated. From Eq. (19), it can be seen that, to calculate the derivative of the SF, the derivative of the negative of the primer vector is needed. The chain rule gives

$$(\boldsymbol{\lambda}_L^T \mathbf{M}_L)' = (\boldsymbol{\lambda}_L')^T \mathbf{M}_L + \boldsymbol{\lambda}_L^T \mathbf{M}_L' \tag{B4}$$

where the derivatives of the costates with respect to the true longitude are

$$(\lambda_p^L)' = \lambda_{L,o}^L \frac{3w_o^2}{2pw^2}, \qquad (\lambda_f^L)' = -2\lambda_{L,o}^L \frac{w_o^2}{w^3}\cos L$$

$$(\lambda_g^L)' = -2\lambda_{L,o}^L \frac{w_o^2}{w^3}\sin L \qquad (\lambda_h^L)' = (\lambda_k^L)' = 0$$

$$(\lambda_L^L)' = -2\lambda_{L,o}^L \frac{w_o^2}{w^3} w' \tag{B5}$$

However, in practice these derivatives of the costates do not need to be calculated, since, as shown in [12],

$$(\boldsymbol{\lambda}_L')^T \mathbf{M}_L = \begin{bmatrix} 0 & -\lambda_{L,o}^L \sqrt{\frac{p}{\mu}} \frac{w_o^2}{w^3} & 0 \end{bmatrix} \tag{B6}$$

All that remains to be calculated to compute the derivative of the primer vector are the derivatives with respect to true longitude of the nonzero elements of $\mathbf{M}_L$, which are

$$(M_{21}^L)' = \sqrt{\frac{p}{\mu}}\cos L, \qquad (M_{31}^L)' = \sqrt{\frac{p}{\mu}}\sin L$$

$$(M_{12}^L)' = -2\sqrt{\frac{p}{\mu}}\frac{pw'}{w^2}$$

$$(M_{22}^L)' = -\sqrt{\frac{p}{\mu}}\left(\sin L + \frac{g}{w} + \frac{j^2 \sin L}{w^2}\right)$$

$$(M_{32}^L)' = \sqrt{\frac{p}{\mu}}\left(\cos L + \frac{f}{w} + \frac{j^2 \cos L}{w^2}\right)$$

$$(M_{23}^L)' = -g(M_{63}^L)', \qquad (M_{33}^L)' = f(M_{63}^L)'$$

$$(M_{43}^L)' = -\sqrt{\frac{p}{\mu}}\frac{s^2(g + \sin L)}{2w^2}$$

$$(M_{53}^L)' = \sqrt{\frac{p}{\mu}}\frac{s^2(f + \cos L)}{2w^2}$$

$$(M_{63}^L)' = \sqrt{\frac{p}{\mu}}\frac{h(f + \cos L) + k(g + \sin L)}{w^2} \tag{B7}$$

Appendix C: Eccentric Longitude System Equations

As with Appendix B, derivations of the results in this Appendix are found in [12]. In this Appendix, prime notation will denote differentiation with respect to eccentric longitude F. Now, from [8], and as given in [12], $\mathbf{D}_F = [0 \quad 0 \quad 0 \quad 0 \quad 0 \quad D_F^F]$ where $D_F^F = n/b$ with the definition $b \equiv 1 - f\cos F - g\sin F$ and where $n = \sqrt{\mu/a^3}$ is the mean motion. Because they are also useful, first and second derivatives of b with respect to eccentric longitude are given here as $b' = f\sin F - g\cos F$ and $b'' = f\cos F + g\sin F = 1 - b$. Using $\mathbf{D}_F$ and Eq. (12), the EL costates during coasting are derived as

$$\lambda_a^F = \lambda_{a,o}^F + \frac{3}{2a}\frac{\lambda_{F,o}^F}{b_o}(F - F_o - b' + b_o')$$

$$\lambda_f^F = \lambda_{f,o}^F - \frac{\lambda_{F,o}^F}{b_o}(\sin F - \sin F_o)$$

$$\lambda_g^F = \lambda_{g,o}^F + \frac{\lambda_{F,o}^F}{b_o}(\cos F - \cos F_o)$$

$$\lambda_h^F = \lambda_{h,o}^F, \qquad \lambda_k^F = \lambda_{k,o}^F, \qquad \lambda_F^F = \lambda_{F,o}^F \frac{b}{b_o} \tag{C1}$$

where, as in Appendix B, the subscript o indicates the initial value of the quantity.

As in Appendix B, for the proposed method of checking the slope at each sampled point, the derivatives with respect to eccentric longitude are now calculated. The derivatives of the EL coasting costates with respect to F are

$$(\lambda_a^F)' = \lambda_{F,o}^F \frac{3}{2a}\frac{b}{b_o}, \qquad (\lambda_f^F)' = -\lambda_{F,o}^F \frac{\cos F}{b_o}$$

$$(\lambda_g^F)' = -\lambda_{F,o}^F \frac{\sin F}{b_o} \qquad (\lambda_h^F)' = (\lambda_k^F)' = 0, \qquad (\lambda_F^F)' = \lambda_{F,o}^F \frac{b'}{b_o} \tag{C2}$$

And, for the sake of writing the dynamic equations during burn arcs, the nonzero elements of $\mathbf{M}_F$ are

$$M_{11}^F = \frac{2\dot{X}_1}{an^2}, \qquad M_{21}^F = -\frac{j}{na^2}\left[\left(\frac{\partial X_1}{\partial g}\right) + \frac{f\beta}{n}\dot{X}_1\right]$$

$$M_{31}^F = \frac{j}{na^2}\left[\left(\frac{\partial X_1}{\partial f}\right) - \frac{g\beta}{n}\dot{X}_1\right]$$

$$M_{61}^F = \frac{1}{na^2 b}\left(-2X_1 + j(g\beta - \sin F)\frac{\partial X_1}{\partial g} + j(f\beta - \cos F)\frac{\partial X_1}{\partial f} - \beta j b'\frac{\dot{X}_1}{n}\right)$$

$$M_{12}^F = \frac{2\dot{Y}_1}{an^2} \qquad M_{22}^F = -\frac{j}{na^2}\left[\left(\frac{\partial Y_1}{\partial g}\right) + \frac{f\beta}{n}\dot{Y}_1\right]$$

$$M_{32}^F = \frac{j}{na^2}\left[\left(\frac{\partial Y_1}{\partial f}\right) - \frac{g\beta}{n}\dot{Y}_1\right]$$

$$M_{62}^F = \frac{1}{na^2 b}\left(-2Y_1 + j(g\beta - \sin F)\frac{\partial Y_1}{\partial g} + j(f\beta - \cos F)\frac{\partial Y_1}{\partial f} - \beta j b'\frac{\dot{Y}_1}{n}\right)$$

$$M_{23}^F = -gM_{63}^F \qquad M_{33}^F = fM_{63}^F$$

$$M_{43}^F = \frac{s^2}{2jna^2}X_1 \qquad M_{53}^F = \frac{s^2}{2jna^2}Y_1$$

$$M_{63}^F = \frac{hY_1 - kX_1}{jna^2} \tag{C3}$$

where $\beta = 1/(1 + j)$ with $j = \sqrt{1 - e^2}$ and $s^2 = 1 + h^2 + k^2$ as defined in Appendix B, and, although somewhat different notation is used in [8], from that work, and as shown in [12],

$$X_1 = a(\cos F - f + g\beta b'), \qquad Y_1 = a(\sin F - g - f\beta b')$$
$$\dot{X}_1 = \frac{an}{b}(g\beta - \sin F) - ang\beta$$
$$\dot{Y}_1 = \frac{an}{b}(-f\beta + \cos F) + anf\beta$$
$$\frac{\partial X_1}{\partial f} = a\left[\frac{fg\beta^3}{1-\beta}b' - 1 - \frac{\sin F}{b}(\sin F - g\beta)\right]$$
$$\frac{\partial X_1}{\partial g} = a\left[\left(\beta + \frac{g^2\beta^3}{1-\beta}\right)b' - \frac{\cos F}{b}(g\beta - \sin F)\right]$$
$$\frac{\partial Y_1}{\partial f} = \frac{\partial X_1}{\partial g} - a\left[\left(2\beta + \frac{(f^2+g^2)\beta^3}{1-\beta}\right)b' + \frac{\beta b'}{b}\right]$$
$$\frac{\partial Y_1}{\partial g} = -\frac{\partial X_1}{\partial f} - a\left(2 + \beta + \frac{1-\beta}{b}\right) \tag{C4}$$

For the purpose of determining derivatives of the SF during coasting, rather than using derivatives of the coasting costates and $\mathbf{M}_F$ and its derivatives, it turns out to be more convenient to write

$$\boldsymbol{\lambda}_F^T \mathbf{M}_F = \boldsymbol{\lambda}_{F,o}^T \mathbf{N}_F \tag{C5}$$

where $\boldsymbol{\lambda}_{F,o}$ is the vector of initial costate values in the EL system. Thus, derivatives are easily calculated from

$$(\boldsymbol{\lambda}_F^T \mathbf{M}_F)^{(i)} = \boldsymbol{\lambda}_{F,o}^T \mathbf{N}_F^{(i)} \tag{C6}$$

where the superscript (i) indicates the ith derivative with respect to F for any order of derivative. All but two nonzero elements of $\mathbf{N}_F^{(i)}$ are

$$N_{11}^{F(i)} = \frac{2\dot{X}_1^{(i)}}{an^2}, \qquad N_{21}^{F(i)} = -\frac{j}{na^2}\left[\left(\frac{\partial X_1}{\partial g}\right)^{(i)} + \frac{f\beta}{n}\dot{X}_1^{(i)}\right]$$
$$N_{31}^{F(i)} = \frac{j}{na^2}\left[\left(\frac{\partial X_1}{\partial f}\right)^{(i)} - \frac{g\beta}{n}\dot{X}_1^{(i)}\right] \qquad N_{12}^{F(i)} = \frac{2\dot{Y}_1^{(i)}}{an^2}$$
$$N_{22}^{F(i)} = -\frac{j}{na^2}\left[\left(\frac{\partial Y_1}{\partial g}\right)^{(i)} + \frac{f\beta}{n}\dot{Y}_1^{(i)}\right]$$
$$N_{32}^{F(i)} = \frac{j}{na^2}\left[\left(\frac{\partial Y_1}{\partial f}\right)^{(i)} - \frac{g\beta}{n}\dot{Y}_1^{(i)}\right] \qquad N_{23}^{F(i)} = -gN_{63}^{F(i)}$$
$$N_{33}^{F(i)} = fN_{63}^{F(i)}, \qquad N_{43}^{F(i)} = \frac{s^2}{2jna^2}X_1^{(i)}$$
$$N_{53}^{F(i)} = \frac{s^2}{2jna^2}Y_1^{(i)}, \qquad N_{63}^{F(i)} = \frac{hY_1^{(i)} - kX_1^{(i)}}{jna^2} \tag{C7}$$

First derivatives of Eq. (C4) with respect to eccentric longitude are

$$X_1' = a[-\sin F + g\beta(1-b)], \qquad Y_1' = a[\cos F - f\beta(1-b)]$$
$$\dot{X}_1' = \dot{X}_2 - \frac{b'}{b}\dot{X}_1, \qquad \dot{Y}_1' = \dot{Y}_2 - \frac{b'}{b}\dot{Y}_1$$
$$\left(\frac{\partial X_1}{\partial f}\right)' = a\left[\frac{fg\beta^3}{1-\beta}(1-b) - \frac{\cos F}{b}(2\sin F - g\beta) + \frac{b'\sin F}{b^2}(\sin F - g\beta)\right]$$
$$\left(\frac{\partial X_1}{\partial g}\right)' = a\left[\left(\beta + \frac{g^2\beta^3}{1-\beta}\right)(1-b) + \frac{\cos^2 F}{b} + \left(\frac{\sin F}{b} + \frac{b'\cos F}{b^2}\right)(g\beta - \sin F)\right]$$
$$\left(\frac{\partial Y_1}{\partial g}\right)' = -\left(\frac{\partial X_1}{\partial f}\right)' + a\left(\frac{1-\beta}{b^2}\right)b'$$
$$\left(\frac{\partial Y_1}{\partial f}\right)' = \left(\frac{\partial X_1}{\partial g}\right)' - a\left[\left(2\beta + \frac{(f^2+g^2)\beta^3}{1-\beta}\right)(1-b) - \frac{\beta}{b} + \frac{\beta j^2}{b^2}\right] \tag{C8}$$

with the definitions

$$\dot{X}_2 \equiv -\frac{an}{b}(g\beta b' + \cos F)$$

and

$$\dot{Y}_2 \equiv \frac{an}{b}(f\beta b' - \sin F)$$

The other two nonzero elements of $\mathbf{N}_F$ are

$$N_{61}^F = \frac{1}{b_o na^2}(Q_{X,0} - 2X_1), \qquad N_{62}^F = \frac{1}{b_o na^2}(Q_{Y,0} - 2Y_1) \tag{C9}$$

with $i = 0$ in the definitions

$$Q_{X,i} \equiv [3(F - F_o - b' + b_o') - j\beta b_o']\frac{\dot{X}_1^{(i)}}{n} + j(f\beta - \cos F_o)\left(\frac{\partial X_1}{\partial f}\right)^{(i)} + j(g\beta - \sin F_o)\left(\frac{\partial X_1}{\partial g}\right)^{(i)}$$
$$Q_{Y,i} \equiv [3(F - F_o - b' + b_o') - j\beta b_o']\frac{\dot{Y}_1^{(i)}}{n} + j(f\beta - \cos F_o)\left(\frac{\partial Y_1}{\partial f}\right)^{(i)} + j(g\beta - \sin F_o)\left(\frac{\partial Y_1}{\partial g}\right)^{(i)} \tag{C10}$$

For the analysis in this paper, it should be noted that the quantity

$$F - b' = E + \omega + \Omega - e\sin E = nt + \omega + \Omega$$

is the mean longitude, which is continually increasing during coasting. Derivatives of the quantities in Eqs. (C10) are

$$Q_{X,i}' = Q_{X,i+1} + 3b\frac{\dot{X}_1^{(i)}}{n}, \qquad Q_{Y,i}' = Q_{Y,i+1} + 3b\frac{\dot{Y}_1^{(i)}}{n} \tag{C11}$$

Thus, the derivatives of $Q_{X,0}$ and $Q_{Y,0}$ are

$$Q_{X,0}' = Q_{X,1} + 3b\frac{\dot{X}_1}{n} = Q_{X,1} + 3X_1', \qquad Q_{Y,0}' = Q_{Y,1} + 3b\frac{\dot{Y}_1}{n} = Q_{Y,1} + 3Y_1' \tag{C12}$$

Finally,

$$N_{61}^{F\prime} = \frac{1}{b_o na^2}(Q_{X,1} + X_1'), \qquad N_{62}^{F\prime} = \frac{1}{b_o na^2}(Q_{Y,1} + Y_1') \tag{C13}$$

References

[1] Glandorf, D. R., "Lagrange Multipliers and the State Transition Matrix for Coasting Arcs," *AIAA Journal*, Vol. 7, No. 2, 1969, pp. 363–365. doi:10.2514/3.5109

[2] Fernandes, S. D. S., "Universal Closed-Form of Lagrangian Multipliers for Coast-Arcs of Optimum Space Trajectories," *Journal of the Brazilian Society of Mechanical Sciences and Engineering*, Vol. 25, No. 4, Oct.–Dec. 2003, pp. 1–14. doi:10.1590/S1678-58782003000400004

[3] Xu, Y., "Enhancement in Optimal Multiple-Burn Trajectory Computation by Switching Function Analysis," *Journal of Spacecraft and Rockets*, Vol. 44, No. 1, Jan.–Feb. 2007, pp. 264–272. doi:10.2514/1.25082

[4] Broucke, R. A., and Cefola, P. J., "On the Equinoctial Orbit Elements," *Celestial Mechanics*, Vol. 5, No. 3, 1972, pp. 303–310. doi:10.1007/BF01228432

[5] Walker, M. J. H., Ireland, B., and Owens, J., "A Set of Modified Equinoctial Orbit Elements," *Celestial Mechanics*, Vol. 36, No. 4, 1985, pp. 409–419. doi:10.1007/BF01227493

[6] Gao, Y., and Kluever, C. A., "Low-Thrust Interplanetary Orbit Transfers Using Hybrid Trajectory Optimization Method with Multiple Shooting," AIAA Paper 2004-5088, 2004.

[7] Coverstone, V., Hartman, C., Herman, A., and Spencer, D., "Orbital Spacecraft Trajectories via Higher Order Differential Inclusion," American Astronautical Society/AIAA Paper 99-128, Feb. 1999.

[8] Kechichian, J. A., "Trajectory Optimization Using Eccentric Longitude Formulation," *Journal of Spacecraft and Rockets*, Vol. 35, No. 3, May–June 1998, pp. 317–326. doi:10.2514/2.3329

[9] Prussing, J. E., and Conway, B. A., *Orbital Mechanics*, Oxford Univ. Press, New York, 1993, pp. 29—38.

[10] Bryson, A. E., and Ho, Y. C., *Applied Optimal Control, Revised Printing*, Taylor and Francis, Philadelphia, 1975, pp. 68–69.

[11] Lawden, D. F., *Optimal Trajectories for Space Navigation*, Butterworths, London, 1963, p. 56.

[12] Jamison, B. R., "Improved Orbit Transfer Switching Function Analysis by an Extended Frequency Study," M.S. Thesis, Univ. of Illinois at Urbana–Champaign, Urbana, IL, Oct. 2007.

[13] Conway, B. A., "An Improved Algorithm Due to Laguerre for the Solution of Kepler's Problem," *Celestial Mechanics*, Vol. 39, No. 2, 1986, pp. 199–211. doi:10.1007/BF01230852